AMERICAN SOCIETY FOR MICROBIOLOGY | mBio®

RESEARCH ARTICLE

An Atypical ABC Transporter Is Involved in Antifungal Resistance and Host Interactions in the Pathogenic Fungus *Cryptococcus neoformans*

Christopher J. Winski,[a] Yuanyuan Qian,[b] Shahriar Mobashery,[b] Felipe H. Santiago-Tirado[a]

[a]Department of Biological Sciences, Eck Institute for Global Health, University of Notre Dame, Notre Dame, Indiana, USA
[b]Department of Chemistry and Biochemistry, Warren Center for Drug Discovery, University of Notre Dame, Notre Dame, Indiana, USA

ABSTRACT ATP-binding cassette (ABC) transporters represent one of the largest protein superfamilies. Functionally diverse, ABC transporters have been implicated in many aspects of microbial physiology. The genome of the human fungal pathogen *Cryptococcus neoformans* encodes 54 putative ABC transporters and most of them remain uncharacterized. In a previous genetic screen for fungal regulators of phagocytosis, we identified an uncharacterized gene, CNAG_06909, that modulates host interactions. This gene encoded a half-size ABC transporter of the PDR-type, and phenotypic studies of a strain with this gene deleted revealed an altered antifungal susceptibility profile, including hypersensitivity to fluconazole (FLC). This gene, which we named *PDR6*, localized to the endoplasmic reticulum (ER) and plasma membrane (PM), and when absent, less ergosterol was observed in the PM. Additionally, we observed that the *pdr6*Δ strain displayed a reduction in secreted polysaccharide capsular material. These changes to the cellular surface may explain the observed increased uptake by macrophages and the reduced intracellular survival. Finally, studies in mice demonstrated that Pdr6 function was required for the normal progression of cryptococcal infection. Taken together, this study demonstrates a novel dual role for PDR transporters in *C. neoformans*, which could represent a potential target for antifungal therapeutics. Furthermore, the atypical half-size transporter encoded by *PDR6* is conserved in many fungal pathogens, but absent in model nonpathogenic fungi. Hence, this study provided a function for this unique group of fungal half-size PDR transporters that, although conserved, remain largely understudied.

IMPORTANCE Conserved across all kingdoms of life, ABC transporters comprise one of the largest protein families. They are associated with multidrug resistance, affecting aspects such as resistance to antimicrobials or anti-cancer drugs. Despite their importance, they are understudied in fungal pathogens. In the environmental fungus *Cryptococcus neoformans*, a leading cause of fungal infections, only a few ABC transporters have been studied. Here, we characterized an atypical, half-size, ABC transporter of the PDR-type, that affected both antifungal resistance and host-pathogen interactions. PDR-type transporters are only present in fungi and plants, and this subgroup of half-size transporters was conserved in fungal pathogens, yet their function was completely unknown. Because the current treatments for cryptococcal infection are suboptimal, understanding the mechanisms of antifungal resistance and the host interactions that drive the infection is critical to improving the management of this disease. Here, we provide insights into these important aspects of cryptococcal pathogenesis.

KEYWORDS ABC transporters, *Cryptococcus neoformans*, antifungal resistance, host-pathogen interactions

Present in every living organism, ATP-binding cassette (ABC) transporters constitute a large superfamily of integral membrane proteins. Functionally, ABC transporters are responsible for the transport of diverse substrates across membranes but have also

Editor J. Andrew Alspaugh, Duke University Medical Center

Address correspondence to Felipe H. Santiago-Tirado, fsantiago@nd.edu.

The authors declare no conflict of interest.

[This article was posted on 21 June 2022 with an incomplete Acknowledgments section. The section was updated in the revised version, posted on 29 July 2022.]

Received 31 May 2022
Accepted 2 June 2022
Published 21 June 2022

been implicated in mRNA translation and peroxisome biogenesis (1, 2). Structurally, ABC transporters contain at least one nucleotide-binding domain (NBD) and one transmembrane domain (TMD), both of which are evolutionary conserved. Most ABC transporters have a domain arrangement of TMD1-NBD1-TMD2-NBD2 ($[TMD\text{-}NBD]_2$) (3). The orientation and molecular architecture of these domains are used to organize ABC transporters into subgroups. The pleiotropic drug resistance (PDR) subgroup, which is present in only fungi and plants, has a reverse configuration $[NBD\text{-}TBD]_2$ (4, 5). Identified and predominantly studied in the nonpathogenic yeast *Saccharomyces cerevisiae*, they remain understudied in pathogenic fungi. This is despite the abundance of fungal PDR proteins and the fact that fungal infections globally kill close to 1.6 million people yearly (6, 7). The few that have been studied mostly act as efflux pumps for xenobiotics, including antifungal drugs. Nonetheless, the sheer number and diversity of PDR genes found in fungal genomes suggest a broad involvement in cellular processes. Moreover, there is a subgroup of half-size PDR transporters (containing only one NBD and TMD) whose function remains unknown. Because all functional PDR transporters studied so far have the typical $[NBD\text{-}TBD]_2$ domain arrangement, these half-size ABC transporters with a [NBD–TMD] topology have been left out of PDR protein phylogenetic studies (4, 5, 8).

Cryptococcus neoformans is an environmental, opportunistic fungal pathogen responsible for over 180,000 deaths annually in the HIV+ population alone (9, 10). Upon inhalation and subsequent lung colonization, *C. neoformans* can disseminate to the central nervous system (CNS) resulting in cryptococcal meningitis, with a mortality rate as high as 81% (10). The high mortality rate is a direct consequence of the complexities associated with cryptococcal pathogenesis coupled with a paucity of effective antifungals. Currently, the most effective treatment for cryptococcal meningitis includes a combinatorial regimen of amphotericin B (AMB) and 5-flucytosine (5-FC). AMB is a fungicidal polyene that targets ergosterol, an essential lipid in the fungal plasma membrane (PM). The pyrimidine 5-FC disrupts DNA/RNA synthesis (11). Notwithstanding the toxicity associated with these agents, they are also costly, which makes them less available to resource-poor countries where the need is highest. Instead, patients in these regions are treated with less effective fluconazole (FLC) monotherapy. FLC is a fungistatic azole that inhibits lanosterol 14α-demethylase, an enzyme in the ergosterol biosynthesis pathway encoded by *ERG11* (12). FLC monotherapy has not only been implicated in higher relapse rates, but several recent studies have reported an increase in the incidence of FLC resistance in *C. neoformans*, making the treatment of cryptococcal meningitis even more challenging (13–16).

Several FLC resistance mechanisms have been reported in *C. neoformans*. These vary from mutations in the *ERG11* gene to heteroresistance due to genome plasticity, including polyploidy, aneuploidy, loss of heterozygosity, and copy-number variation (17–20). Additionally, the overexpression of ABC efflux pumps has been implicated in FLC resistance (21). There are 54 putative ABC transporters in the *C. neoformans* genome and only a few have been characterized. The roles of *C. neoformans AFR1*, *PDR5* (also called *AFR2*), and *MDR1* as azole efflux pumps have been well documented, where *AFR1* functions as the major pump and *AFR2* and *MDR1* provide additive roles in the management of FLC stress (22–25). The function of most of the ABC transporters encoded in the *C. neoformans* genome remains unknown. In an earlier report on fungal regulators of phagocytosis, we identified an uncharacterized gene, CNAG_06909, as a modulator of the fungal-host interaction (26). Here, we demonstrated that CNAG_06909 encodes a half-size PDR-transporter and that disruption of the gene resulted in hypersensitivity to FLC. Following nomenclature guidelines for the field (27), we have designated the gene as pleiotropic drug resistance-6 (*PDR6*) because it does not have a direct ortholog in the model yeast *S. cerevisiae* and the molecular architecture is consistent with the PDR subgroup of ABC transporters (see Text S1 for more details). We showed that Pdr6 does not function as an FLC efflux pump, but its deletion resulted in decreased levels of ergosterol in the PM accompanied by mild thermosensitivity and decreased secretion of capsular material. These phenotypes are unique to *PDR6* because they were not observed in the previously

characterized ABC transporters. Furthermore, the *pdr6*Δ strain exhibited diminished intracellular survival *in vitro* and is attenuated in a murine model of infection. When the gene was expressed in model yeast, it localized to the ER and PM, consistent with a role in ergosterol synthesis/transport. Notably, this study provided a function for the group of unconventional, yet conserved, half-size PDR transporters, which has remained largely obscure. These studies highlighted the importance of fungal PDR-type transporters and broaden our understanding of the specialization of ABC transporters in microbial pathogens.

RESULTS

***C. neoformans PDR6* is a member of a conserved group of half-size PDR transporters.** Present in only fungi and plants, PDR-type ABC transporters represent a unique subset of proteins primarily implicated in drug resistance and detoxification (4). Although fungal PDR-type transporters closely resemble mammalian ABCG transporters, which are half-size, only the full-size fungal PDR proteins have been analyzed and studied (5, 8, 28). Given that *C. neoformans PDR6* is half-size, we performed a phylogenetic analysis to determine how widespread *PDR6* sequences are in the fungal kingdom (Fig. 1A). All fungi belonging to the Pezizomycotina subphylum, and all the pathogenic fungi analyzed have a *PDR6* ortholog, implicating *PDR6* in fungal pathogenesis in many subphyla. Regardless of the presence of a *PDR6* ortholog, all the PDR-type ABC transporter genes from the organisms in Fig. 1A were used to construct a global phylogenetic tree (Fig. 1B). Analysis of the fungal PDR genes showed the presence of seven major clades. Clade I was the largest and included *S. cerevisiae PDR5*, *PDR10*, *PDR15*, and *C. neoformans PDR5* (referred to by its alias *AFR2*). Clade II was the smallest and contained sequences that were homologous to *S. cerevisiae PDR12*, *PDR18,* and *SNQ2*. Clade III sequences were absent in Saccharomycotina but contain *C. neoformans AFR1*. *S. cerevisiae PDR11* and *AUS1* represent the genes in clade IV. Clades I, II, III, IV, and VIa all contained full-length *PDR* genes, whereas clades V and VIb represented atypical groups of PDR genes that only encoded one nucleotide-binding domain (NBD) and one transmembrane domain (TMD). *S. cerevisiae ADP1* was representative of the genes in clade V that all contained an NBD and TMD with an additional unique sequence (most commonly an EGF domain). *C. neoformans PDR6* and the 11 other half-size PDR genes in clade VIb represented a completely uncharacterized group of fungal genes with no known function. Interestingly, the fungi represented in clade VIb were all plant or animal pathogens, again suggestive that *PDR6* and its orthologs may be implicated in fungal virulence. Topology prediction by CAMPS (29) showed that *C. neoformans PDR6* encoded a 626 amino acid half-size transporter, with a single NBD containing characteristic Walker A, Walker B, and ABC motif features followed by a single TMD, composed of six transmembrane helices (Fig. 1C). These analyses show that *C. neoformans PDR6* encodes a half-size PDR-type ABC transporter that is evolutionarily conserved, with orthologs present in all fungal pathogens that we analyzed and contains all the features of a functional ABC transporter.

Deletion of *PDR6* affects resistance to azoles and the drug profile of other antifungals. Given that cryptococcal PDR-type ABC transporters Afr1 and Afr2 have been implicated in the efflux and resistance of antifungal compounds (23–25), we hypothesized that Pdr6 would function similarly. To assess the function/specificity of Pdr6, we used a *C. neoformans* strain lacking the *PDR6* gene (*pdr6*Δ) and tested its growth on FLC gradient plates and Etest strips (Fig. 2A), and performed broth microdilution assays to measure the minimal-inhibitory concentrations (MICs) of several related compounds (Fig. 2B to G and Table 1). Compounds included five azole-class antifungals (FLC), itraconazole (ITC), voriconazole (VRC), ketoconazole (KTC), and posaconazole (PSC), one polyene-class antifungal (amphotericin B [AMB]), one DNA/RNA synthesis inhibitor (5-fluorocytosine [5-FC]), one protein-synthesis inhibitor (cycloheximide [CHX]), one antineoplastic agent (nocodazole), two other xenobiotics (berberine [BER], and paraquat [PQ]), one superoxide generator (menadione), and one echinocandin-class antifungal (caspofungin [CSF]). In addition to the *pdr6*Δ mutant strain, we used the *afr1*Δ, *afr1*Δ/*afr2*Δ/*mdr1*Δ, and *erg3*Δ strains as controls because all have displayed increased FLC susceptibility (24, 30).

Among the compounds tested, we found that the *pdr6*Δ mutant displayed a

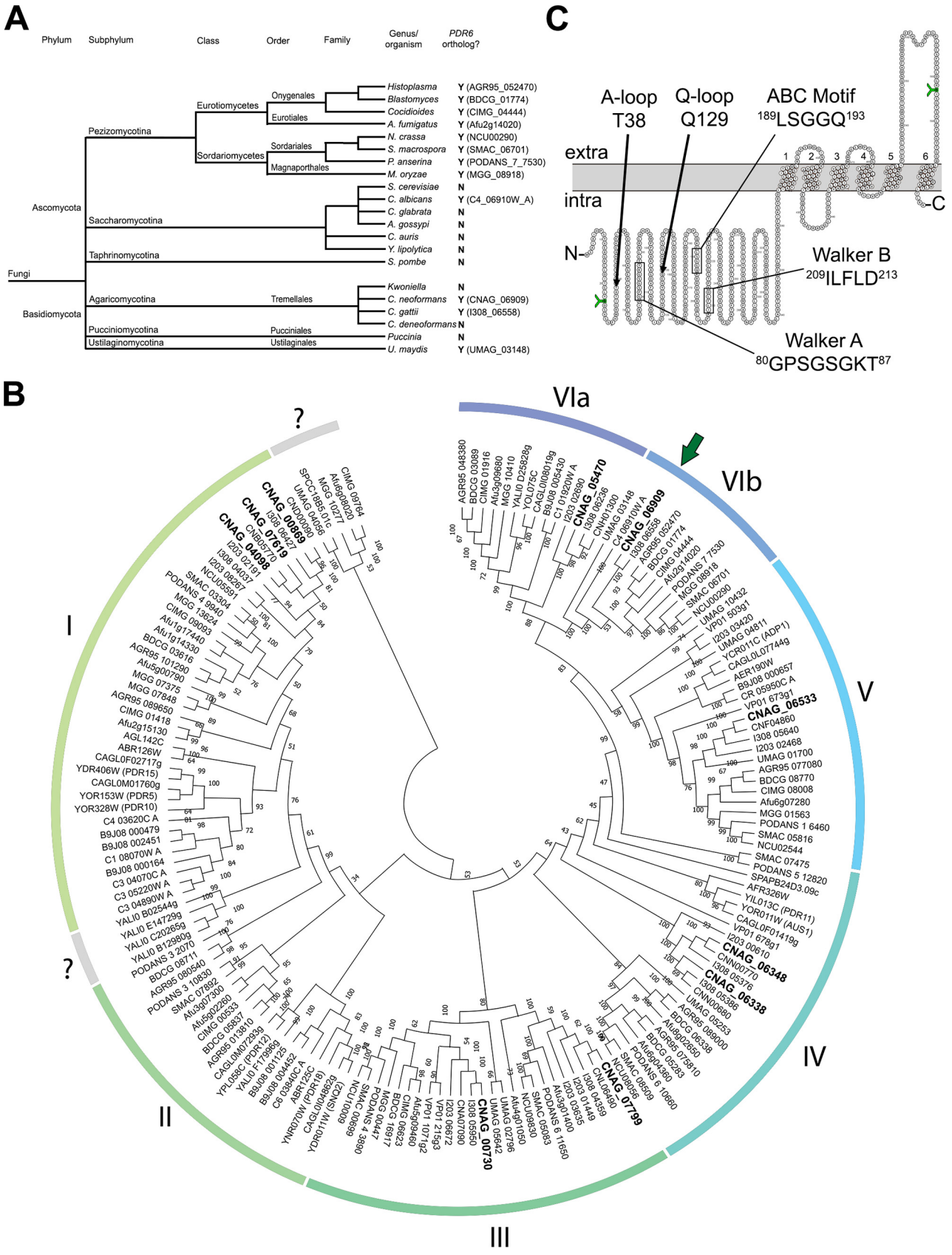

FIG 1 *PDR6* contains all the features of a PDR-type ABC transporter and is conserved in a subset of fungal pathogens. (A) Cladogram showing the fungal distribution of *PDR6* orthologs in the two main phyla. When present, the gene name of the ortholog is stated within parentheses. (B) Global

(Continued on next page)

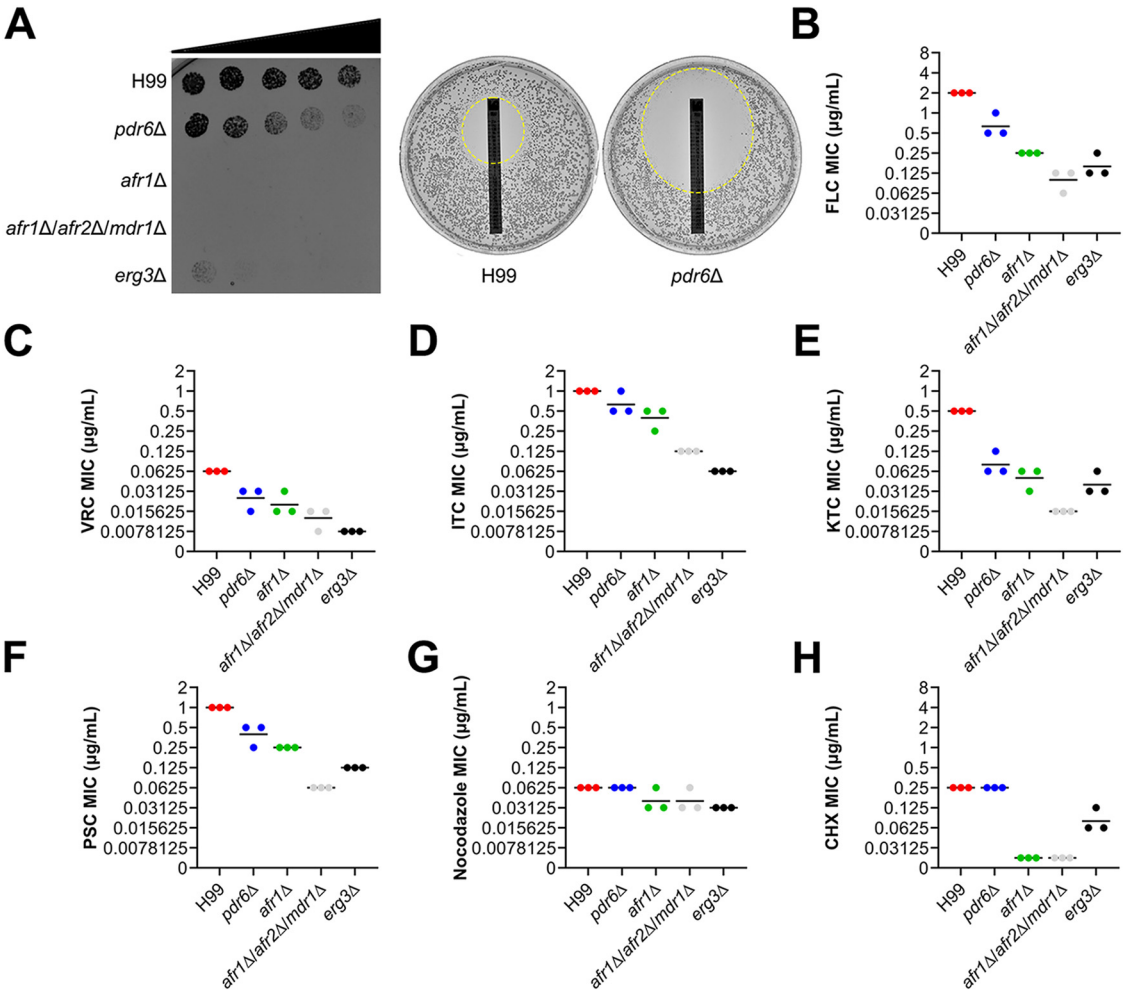

FIG 2 *PDR6* is involved in azole resistance. (A) The *pdr6*Δ mutant showed increased sensitivity to FLC gradient plates and Etest strips. (Left) 500 cells of the indicated strains were spotted across an RPMI 1640 agar plate with a gradient of FLC concentration (denoted by a black triangle). The gradient goes from near zero on the left side to a peak concentration of 4 μg/mL on the right side of the plate. (Right) FLC Etest strips were applied to RPMI 1640 agar plates with 2×10^5 cells of the indicated strain. The zone of inhibition is highlighted with a dashed circle, and the MICs of H99 and the *pdr6*Δ mutant were 6 and 0.38 μg/mL, respectively. These plates were incubated for 72 h at 30°C. (B to H) Quantitative broth microdilution assays were used to compare MICs of several antifungal compounds in the WT and the indicated mutant strains. The CLSI M27-A3 reference method was repeated three times for each compound and the bars represent the average of the MICs. The details for each strain's MICs are listed in Table 1. FLC, fluconazole; VRC, voriconazole; ITC, itraconazole; KTC, ketoconazole; PSC, posaconazole; CHX, cycloheximide.

hypersensitive phenotype specifically toward the azole class antifungals, albeit not as drastic as the *afr1*Δ, *afr1*Δ/*afr2*Δ/*mdr1*Δ, or *erg3*Δ strains (Fig. 2 and Table 1). The MICs of the non-azole compounds in the *pdr6*Δ strain were comparable to those of the H99 WT, suggesting a specific role of Pdr6 in azole resistance. Additionally, previous studies have shown a relationship between environmental pH and antifungal efficacy (31), so we performed FLC susceptibility assays under alkaline and acidic conditions (Fig. S1A and B). Regardless of the pH, the MICs of the WT and *pdr6*Δ strains displayed similar trends indicating that *PDR6* functions in a pH-independent manner.

Given the increase in azole susceptibility by the *pdr6*Δ mutant, we performed checker-

FIG 1 Legend (Continued)

phylogenetic tree showing the evolutionary relationships of PDR-type ABC transporters in 21 fungal organisms. Gene names are given in NCBI nomenclature. The tree was generated by the maximum likelihood method using MEGA-X and confidence values determined from 500 bootstraps with bootstrap scores shown at all nodes. The tree shown is the bootstrap consensus tree. Analysis revealed VI major clades with *C. neoformans PDR6* housed in clade VIb (denoted by dark green arrow). The 10 PDR-type transporters in *C. neoformans* are in bold font and are listed in Text S1. (C) Topology prediction of Pdr6 protein by Computational Analysis of the Membrane Protein Space (CAMPS) software showing the domain arrangement of the half-size PDR transporter. The 5 main consensus motifs of the nucleotide-binding domain (NBD) are depicted. The residues in green with a green 'Y' were predicted N-glycosylation sites.

TABLE 1 MICs of antifungals and xenobiotics.[a]

	MICs (μg/mL)													
Strain	FLC	ITC	VRC	KTC	PSC	AMB	5-FC	CHX	NOC	BER	PQ	TSA	MEN	CSF
H99	2	1	0.0625	0.5	1	4	2	0.25	0.0625	8	12.5	2	16	32
*pdr6*Δ	0.5–1	0.5–1	0.0156–0.0312	0.0625–0.125	0.25–0.5	4	4	0.25	0.0625	8	12.5	2	16	64
*afr1*Δ	0.25	0.25–0.5	0.0156–0.0312	0.0312–0.0625	0.25	4	2	0.0156	0.0312–0.0625	8	12.5	0.5	16	64
*afr1*Δ/*afr2*Δ/*mdr1*Δ	0.0625–0.125	0.125	0.0078–0.0156	0.0156	0.0625	4	4	0.0156	0.0312–0.0625	8	12.5	0.5	8	64
*erg3*Δ	0.125–0.25	0.0625	0.0078	0.0312–0.0625	0.125	4	2	0.0625–0.125	0.0312	0.5	3.125	0.5	16	32

[a]Values given are the range of MICs obtained from at least three independent experiments. FLC, fluconazole; ITC, itraconazole; VRC, voriconazole; KTC, ketoconazole; PSC, posaconazole; AMB, amphotericin B; 5-FC, 5-fluorocytosine; CHX, cycloheximide; NOC, nocodazole; BER, berberine; PQ, paraquat; TSA, trichostatin A; MEN; menadione; CSF, caspofungin.

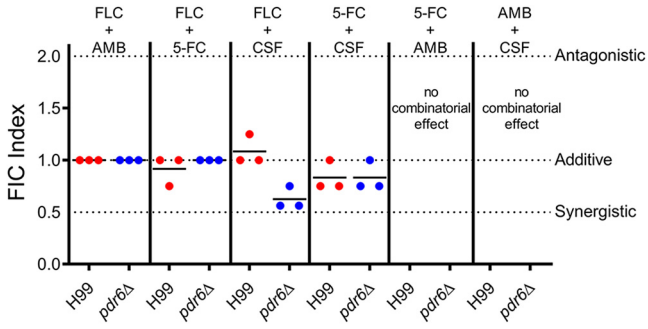

FIG 3 Combinatorial FLC+CSF treatment have an additive effect in *pdr6*Δ mutant. Checkerboard assays assessed changes in drug combinatorial activity in H99 and *pdr6*Δ strains. The combination of FLC+CSF resulted in average sums of FIC of 1.083 and 0.625 in the H99 and *pdr6*Δ strains, respectively. Calculations indicate an additive effect trending into synergistic in the absence of *PDR6*. Checkerboard assays were repeated three times for each combination and black bars represent the average sum of FIC.

board assays with four common antifungals, FLC, AMB, 5-FC, and CSF (Fig. 3). Interestingly, we found that FLC coupled with CSF functions differently in the *pdr6*Δ strain compared to the WT. The combination worked strongly in an additive manner in the *pdr6*Δ strain but showed minimal combinatorial effects in the WT. This finding was unexpected given that CSF is ineffective at treating cryptococcal infections. Additional experimentation is required to explain the observed finding. Nonetheless, these data show that *PDR6* is involved in azole resistance, is not affected by pH, and can alter antifungal combinatorial behaviors. All these results were confirmed using three independently recreated *pdr6*Δ mutants (Fig. S1C and Materials and Methods).

Deletion of *PDR6* does not affect drug accumulation. The increased azole susceptibility of the *pdr6*Δ mutant led us to hypothesize that Pdr6 could function as an efflux pump, similar to many of the characterized fungal PDR transporters. Rhodamine 6G (R6G) and Nile Red (NR) are fluorescent xenobiotics that have been used as generic probes to measure ABC transporters' efflux activity (32, 33). To determine if Pdr6 functions as an efflux pump, we measured the intracellular accumulation of R6G and NR by flow cytometry (Fig. 4A). Surprisingly, no difference was observed in the mean fluorescent intensity (MFI) values of either R6G or NR in the *pdr6*Δ mutant, compared to the WT. In contrast, the *afr1*Δ and *afr1*Δ/*afr2*Δ/*mdr1*Δ strain accumulated high levels of these xenobiotics. We reasoned that Pdr6 may not recognize R6G or NR and potentially, Pdr6 is strictly an azole-specific transporter. To test this, we synthesized a dansyl amide labeled-FLC molecule, termed Probe 1 (Fig. 4B, left), that has been used to visualize the intracellular localization of FLC in *Candida albicans* (34). Although the modification of FLC with dansyl amide affected its antifungal activity, the strains more sensitive to FLC were also more sensitive to Probe 1, indicating a similar mechanism of action (Fig. 4B, right). Consistently, the intracellular accumulation of Probe 1 was significantly increased in the *afr1*Δ and *afr1*Δ/*afr2*Δ/*mdr1*Δ strains (Fig. 4C). However, there was no difference in the intracellular accumulation of Probe 1 between the *pdr6*Δ strain and WT, suggesting that Pdr6 is not a major efflux pump for FLC and instead affects azole activity by a different mechanism. We also used light microscopy to assess the intracellular localization and accumulation/fluorescent intensity of Probe 1 between strains and no differences in location were observed, while fluorescent intensity values supported the findings above (unpublished data). To provide definitive support that Pdr6 is not acting as an FLC-specific efflux pump, we directly measured the accumulation of FLC using a liquid chromatography-mass spectrometry (LC-MS)-based FLC accumulation assay (Fig. 4D). We found that the *pdr6*Δ mutant once again displayed levels comparable to the WT, while the *afr1*Δ/*afr2*Δ/*mdr1*Δ positive-control strain accumulated significant amounts of FLC. Taken together, these data support that Pdr6 is not functioning as a drug-efflux pump and that the hypersensitivity to azole antifungals in the *pdr6*Δ strain is not due to increased accumulation of these drugs.

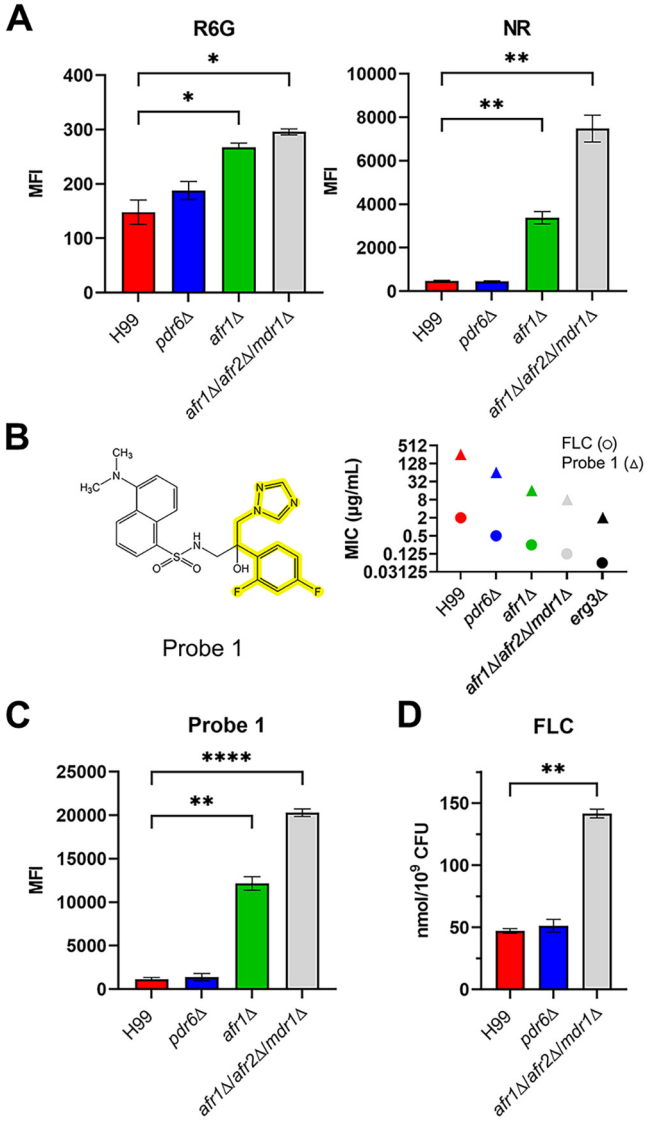

FIG 4 Deletion of *PDR6* does not affect the intracellular accumulation of fluorescent reporters or FLC. (A) H99 and indicated deletion strains were incubated with 10 μM R6G or 7 μM NR for 30 min at 30°C and the accumulation of the reporter in the cells was analyzed by flow cytometry as described in Materials and Methods. (B) Chemical structure of Probe 1 with FLC backbone highlighted (left). Broth microdilution assays were performed to compare the MICs of FLC with Probe 1 (right). Regardless of strain, a 128-fold increase was observed in the MICs of Probe 1 compared to FLC. Microdilution assays were repeated three times and shown are the results from one representative experiment. (C) Indicated strains were incubated with 10 μg/mL of Probe 1 and accumulation was assessed by flow cytometry as above. (D) Accumulation of FLC was assessed in H99 and deletion strains using LC-MS/MS. Strains were incubated with 16 μg/mL of FLC for 30 min at 30°C. All values represent the mean ± SEM from three to four independent experiments. Significance was determined using one-way analysis of variance (ANOVA) compared to H99 (Brown-Forsythe and Welch's corrected); *, $P < 0.05$; **, $P < 0.01$; ****, $P < 0.0001$.

***PDR6* is involved in ergosterol trafficking.** To mechanistically explain Pdr6's contribution to antifungal resistance, we next considered azoles' mode of action. It is well documented that the target of azoles is Erg11, an enzyme in the ergosterol biosynthesis pathway (18, 35). Disruptions to the ergosterol metabolic pathway can result in the accumulation of sterols, which have been implicated in both diminished and increased effectiveness of azole compounds (30, 36). We, therefore, hypothesized that the azole resistance phenotype might be a result of *Pdr6*'s involvement in ergosterol transport. To quantify ergosterol content in the cryptococcal PM, we used filipin, a sterol-binding fluorescent dye (Fig. 5). We found a significant difference in fluorescence between the WT and the *pdr6*Δ mutant. Specifically, the deletion of *PDR6* resulted in decreased

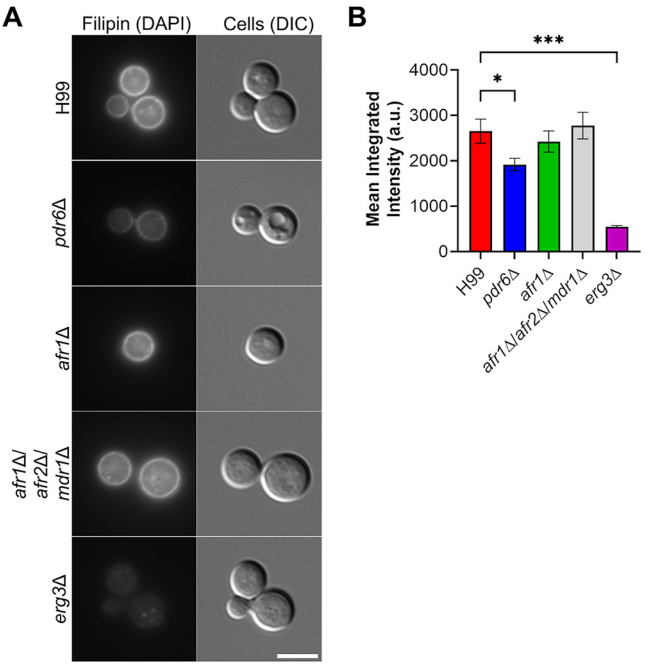

FIG 5 *pdr6*Δ mutant displays reduced sterol content. To assess sterol content in WT and other mutant strains, the cells were incubated with 5 μg/mL Filipin III for 5 min at 30°C and visualized microscopically (left). Scale bar, 5 μm. Quantification of fluorescence using a Cell Profiler pipeline (right). Values represented are the mean ± SEM of 3 to 4 independent experiments where $n = 50$ cells per experiment. Significance was determined using one-way ANOVA with multiple comparisons (Brown-Forsythe and Welch's corrected); *, $P < 0.05$; ***, $P < 0.001$.

fluorescence, suggesting that less sterol is present and that Pdr6 plays a role in either the synthesis of sterols or their trafficking; ABC transporters have been implicated in the latter (1, 37, 38), supporting a potential role for Pdr6 in ergosterol transport to the PM. Notably, neither the *afr1*Δ nor *afr1*Δ/*afr2*Δ/*mdr1*Δ strains exhibited reductions in filipin staining, indicating that the reduced sterol is specific for *pdr6*Δ. As a control, we used *erg3*Δ strain, which was expected to have low levels of ergosterol and, consistently, had almost no detectable staining. We further corroborated the quantitative microscopy results using a fluorescent plate reader, confirming that the *pdr6*Δ mutant has reduced overall ergosterol, compared to the WT (unpublished data). These findings provide context for the previously observed antifungal phenotype and demonstrate that the *pdr6*Δ strain has an altered PM with less ergosterol, consistent with a role of *PDR6* in ergosterol transport/trafficking. Lastly, an indirect role of *PDR6* in azole resistance is supported by the fact that the presence of FLC does not affect the expression of *PDR6* (Fig. S2A), while growth under host-like conditions (DMEM, 37°C, 5% CO_2) induce a rapid and sustained increase in transcript levels (Fig. S2B). Ergosterol is essential for thermotolerance and survival inside mammalian hosts (38), hence, if *PDR6* were involved in ergosterol transport, then it would be expected to be overexpressed under host-like conditions.

Pdr6 localizes to the ER and PM. To better understand the function of Pdr6, we generated a C-terminally tagged *PDR6*-GFP integrative construct under the control of the *PDR5* promoter and introduced it into the *S. cerevisiae* strain ADΔΔ (39, 40). This strain is missing seven major endogenous ABC transporters and expresses a mutant Pdr1 transcription factor, driving the overexpression of PDR genes. This strain allows for the visualization of Pdr6 localization and a more direct assessment of efflux activity, provided cryptococcal Pdr6 would be the only major PDR protein in the cell. Visualization of the ADΔΔ+Pdr6-GFP strain revealed clear perinuclear and peripheral staining, characteristic of the yeast endoplasmic reticulum (ER) (Fig. 6A). Similarly, a control ADΔΔ strain expressing Afr1-GFP, a full-length PDR-type transporter, displayed

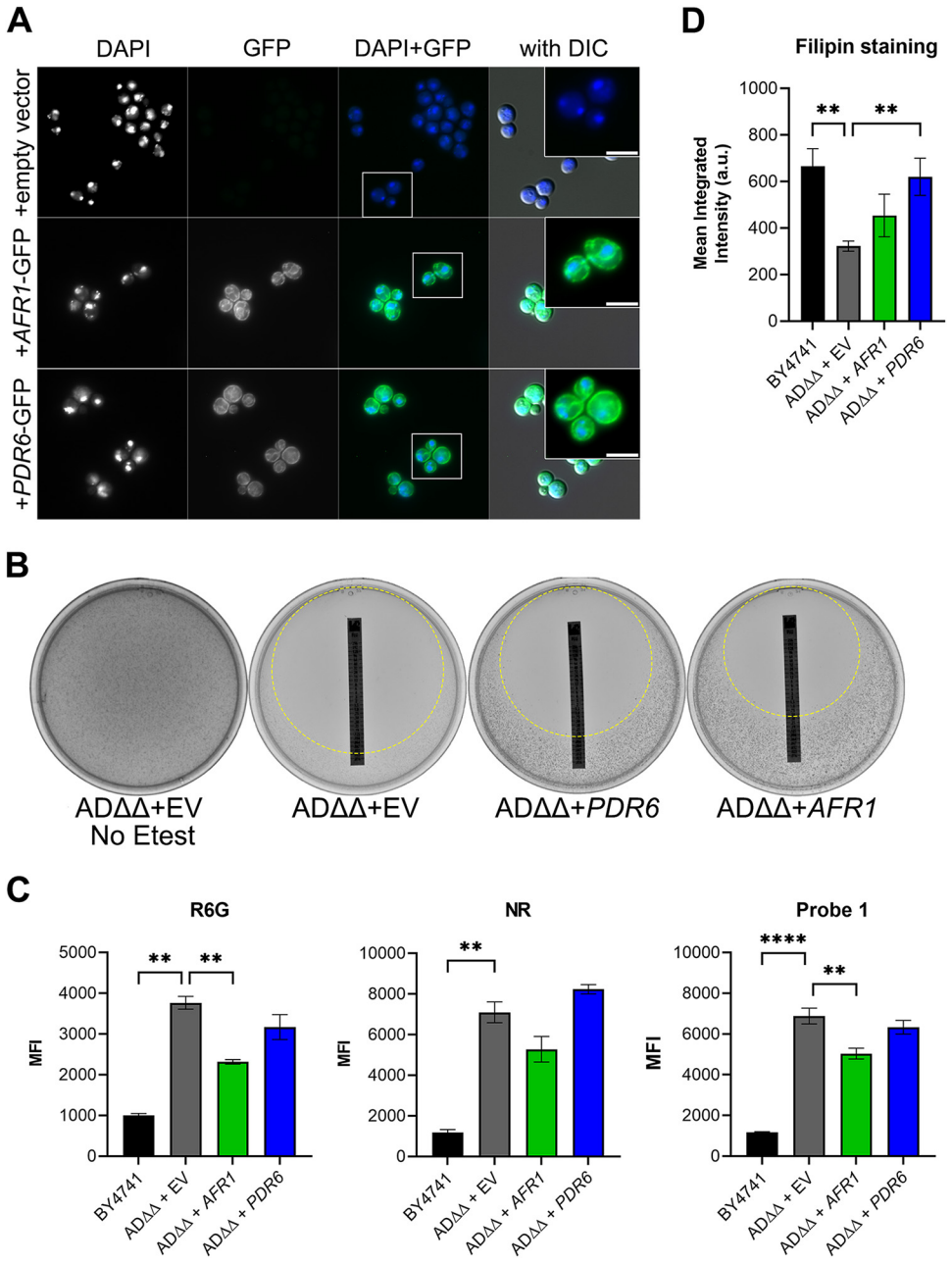

FIG 6 Pdr6 localizes to the ER and PM in *S. cerevisiae* but do not affect intracellular drug accumulation. (A) Visualization of *S. cerevisiae* ADΔΔ expressing *C. neoformans PDR6*-GFP, *AFR1*-GFP, or empty vector. DAPI staining was included to highlight the perinuclear staining. The GFP-tagged protein localization is consistent with the ER and PM. Scale bar, 3.8 μm. (B) Growth of the various ADΔΔ strains was assessed using FLC Etest strips in RPMI plates. Strains expressing *PDR6* (MIC = 0.25 μg/mL) and *AFR1* (MIC = 0.75 μg/mL) display increased resistance to FLC compared to empty vector control (MIC = 0.064 μg/mL) but the strain expressing *AFR1* was most resistant. Plates were incubated at 30°C for 96 h and imaged. The zones of inhibition are highlighted with a dashed circle. (C) Accumulation of the indicated reporters was assessed by flow cytometry as described in Fig. 4. There was no difference between the accumulated drugs in the empty vector control and the strain expressing *PDR6*-GFP. Values represent the mean ± SEM of at least 3 independent experiments. Significance was determined using one-way ANOVA with multiple comparisons (Brown-Forsythe and Welch's corrected); **, $P < 0.01$; ****, $P < 0.0001$. (D) Quantification of sterol content in transformed ADΔΔ strains and BY4741 control. The ADΔΔ + *PDR6* displayed increased filipin staining compared to the ADΔΔ control and ADΔΔ + *AFR1* but are indistinguishable from the WT BY4741 strain. Log-phase cells were incubated with filipin and imaged/quantified as described in Fig. 5. Values represent the mean ± SEM where $n = 50$. Significance was determined using one-way ANOVA with multiple comparisons (Brown-Forsythe and Welch's corrected); **, $P < 0.01$.

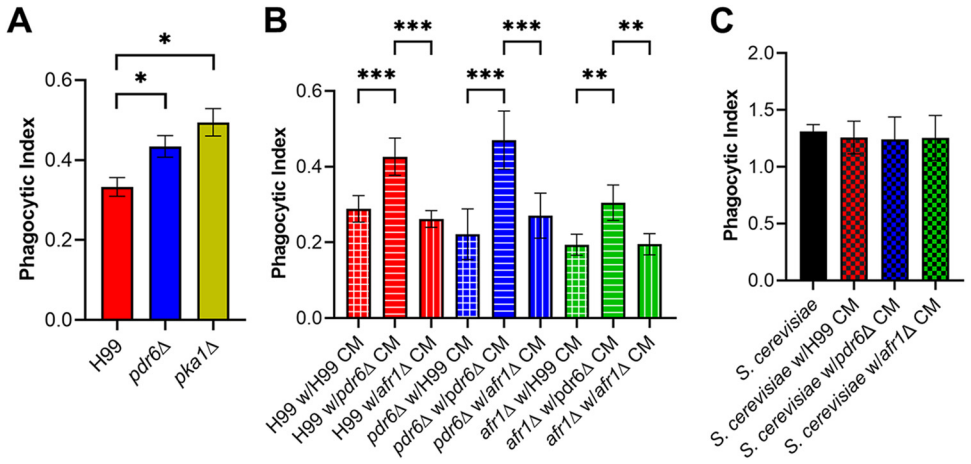

FIG 7 The *pdr6*Δ mutant conditioned medium (CM) increases the phagocytosis of other cryptococcal strains by host macrophages. (A) Uptake assays of WT and deletion strains were performed to determine phagocytic indices of respective strains. The *pdr6*Δ mutant displayed increased uptake compared to the H99 strain. The *pka1*Δ cells were used as a positive control. Stained and opsonized log-phase cells were incubated for 1 h with THP-1 cells and imaged using automated microscopy. Values represent the mean ± SEM from three independent experiments. (B) An uptake assay using CM from cryptococcal strains was performed. CM was obtained by centrifugation and filtration of supernatants from 5-day cultures incubated at 37°C and 5% CO_2 in RPMI 1640 medium. The *pdr6*Δ CM altered the phagocytic uptake values of the WT strain and vice versa, whereas the *afr1*Δ CM had no effect. Values represent the mean ± SD of a representative experiment from three independent experiments. (C) Uptake assays with CM were performed as in (B) but using *S. cerevisiae* strain BY4741. BY4741 was easily phagocytized by THP-1 cells under all conditions. Significance was determined using one-way ANOVA with multiple comparisons (Brown-Forsythe and Welch's corrected), *, $P < 0.05$; **, $P < 0.01$; ***, $P < 0.001$.

comparable localization patterns consistent with the ER and PM (Fig. 6A). No GFP fluorescence was seen in the strain transformed with an empty vector (Fig. 6A).

***PDR6* expression does not restore efflux activity but increases sterol staining in the ADΔΔ strain.** Using the same set of strains as above, we measured FLC susceptibility with Etest strips. The strain expressing Afr1-GFP, a known FLC efflux pump, exhibited a 12-fold increase in MIC (MIC = 0.75 μg/mL) over the ADΔΔ+empty vector control (MIC = 0.064 μg/mL; Fig. 6B). In contrast, the ADΔΔ+Pdr6-GFP strain exhibited a modest increase with a MIC of 0.25 μg/mL, resulting in a 4-fold increase over the control but a 3-fold decrease compared to the ADΔΔ+Afr1-GFP strain. If this small increase in MIC was due to Pdr6-efflux activity, we should be able to measure it using the flow cytometry assay described above. As shown in Fig. 6C, no differences were seen in the amounts of accumulated drugs between the ADΔΔ+empty vector control and the strain expressing *PDR6*-GFP. In contrast, expression of *AFR1*-GFP resulted in a significant decrease in the levels of R6G and Probe 1, albeit not to the levels seen in the WT BY4741 control strain. The decrease in NR was not statistically significant, but a clear downward trend was also observed in the ADΔΔ+Afr1-GFP strain. Next, given the filipin-staining results shown in Fig. 5, we reasoned that the small MIC increase seen could be due to the potential role of Pdr6 in ergosterol transport. To test this, we subjected the set of ADΔΔ strains to filipin staining and analysis as above. Consistently, the ADΔΔ strains with an empty vector or expressing Afr1-GFP had the lowest PM fluorescence, while the ADΔΔ+Pdr6-GFP had fluorescence that was indistinguishable from the WT control (Fig. 6D). All these results, together with the localization of Pdr6-GFP, suggest that the role of Pdr6 in azole resistance stems from effects on ergosterol synthesis and/or transport and not from acting as a specific FLC efflux pump.

***PDR6* influence interaction with host macrophages.** Alveolar macrophages represent the first line of defense against cryptococcal infections, and the complex fungal-phagocyte interaction ultimately determines the course of infection and patient outcome (41). We initially identified *PDR6* in a screen for fungal regulators of phagocytosis (26). We used the same automated high-content imaging method to quantify the phagocytic index (PI) of the library's *pdr6*Δ strain and the recreated strains by a human monocytic cell line (THP-1) (Fig. 7A and Fig. S1D). In agreement, the original and recreated *pdr6*Δ mutants were all

phagocytosed more readily than the WT, providing evidence that changes in phagocytosis are a direct result of loss of *PDR6* function. The *pka1*Δ strain served as a high-uptake positive control (26). This observation begs the question of how the deletion of an atypical PDR-type ABC transporter was affecting the cryptococcal-host interaction. We first tested if the absence of *PDR6* affected the cryptococcal capsule. The *pdr6*Δ mutant was able to generate a capsule comparable to the WT, indicating that *PDR6* is not involved in capsule formation (Fig. S2C). We next assessed if there were any defects in cell wall structure by growing *pdr6*Δ, WT, *erg3*Δ, *afr1*Δ, and *afr1*Δ/*afr2*Δ/*mdr1*Δ under cell wall-stress conditions (Fig. S2D). All strains (except for *erg3*Δ) grew under the tested conditions, and melanized normally, suggesting that there were no defects in the cell wall (Fig. S2D and E). Finally, we hypothesized that *PDR6* was involved in the secretion/efflux of an immunomodulatory factor and thus influencing host interactions. To test this idea, we performed similar uptake assays as previously described, but used strain-specific conditioned media (CM) during the cryptococcal-macrophage coincubation. The thought process being that if *PDR6* is responsible for the release of an immunomodulatory compound, then the CM from the *pdr6*Δ strain should influence the uptake of the WT to increase the PI values, whereas the CM from the WT should decrease the PI values of the *pdr6*Δ strain. As shown in Fig. 7B, there were significant differences in phagocytosis dependent on the source of the CM. Specifically, the incubation of the WT with *pdr6*Δ CM increased uptake ~2-fold, while the incubation of the *pdr6*Δ strain with WT CM decreased uptake back to WT levels. Notably, the use of CM from the *afr1*Δ mutant had no significant impact on the PI values of either WT or *pdr6*Δ strains. To test if this effect was specific to cryptococcal cells or impacted all phagocytic cargo, we carried out the same assay with nonpathogenic *S. cerevisiae* (Fig. 7C). The host cells were able to phagocytize a significant portion of this yeast regardless of the CM used. This suggested that *PDR6* is involved in the release of an immunomodulatory factor that is present in the media and significantly impacts the phagocytosis of cryptococcal cells by host phagocytes. Taken together, these data confirm that the *pdr6*Δ mutant is recognized and phagocytosed more avidly than the WT strain and that the deletion of *PDR6* alters the secretion/efflux of cryptococcal immunomodulatory compounds.

***PDR6* is involved in capsular shedding and adherence.** To investigate in more detail how *PDR6* is altering the cryptococcal-phagocyte interaction, we focused on the polysaccharide capsule. Primarily composed of glucuronoxylomannan (GXM) and glucuronoxylomannogalactan (GXMGal), the capsule is known to be secreted/shed constitutively. This secreted capsule plays a central role in virulence by acting as an antiphagocytic factor, providing protection against host stressors, and modulating the host immune response (42, 43). We wondered if the release/secretion of the capsule into the surrounding environment is altered in the *pdr6*Δ mutant. To test this, we analyzed the amount of shed capsule by electrophoresis and immunoblotting using anti-GXM antibodies (Fig. 8A) (44). Quantification of the immunoblots (Fig. 8A and Fig. S2G) showed that the *pdr6*Δ mutant shed less capsule compared to the WT in both DMEM and YNB medium, and this was significantly more pronounced in DMEM (Fig. 8A). Notably, there were no differences in shed capsule between the *afr1*Δ, *afr1*Δ/*afr2*Δ/*mdr1*Δ, or *erg3*Δ strains and the WT, indicating that this phenotype is unique to the Pdr6 transporter and not related to low levels of ergosterol. The acapsular strain *cap59*Δ was used as a control. This observed defect in capsule shedding could explain the phagocytosis phenotype, but to further test if there are functional consequences associated with this defect, we performed biofilm/adherence assays (Fig. 8B). Previous studies have shown that shed GXM is essential for the formation of cryptococcal biofilms (45–47). Consistently, we found a similar trend where the *pdr6*Δ strain formed weaker/fewer biofilm structures compared to the WT, as measured by biomass quantification using an anti-GXM antibody. Identical results were obtained by metabolic quantification using XTT reduction assays (unpublished data). Taken together, these data suggest that *PDR6* is implicated in the shedding of the polysaccharide capsule, affecting both phagocytosis by host cells and biofilm formation.

***PDR6* function is required for *in vitro* and *in vivo* virulence.** Given the altered host interactions exhibited by the *pdr6*Δ mutant, its mild thermotolerance (Fig. S2F), and the

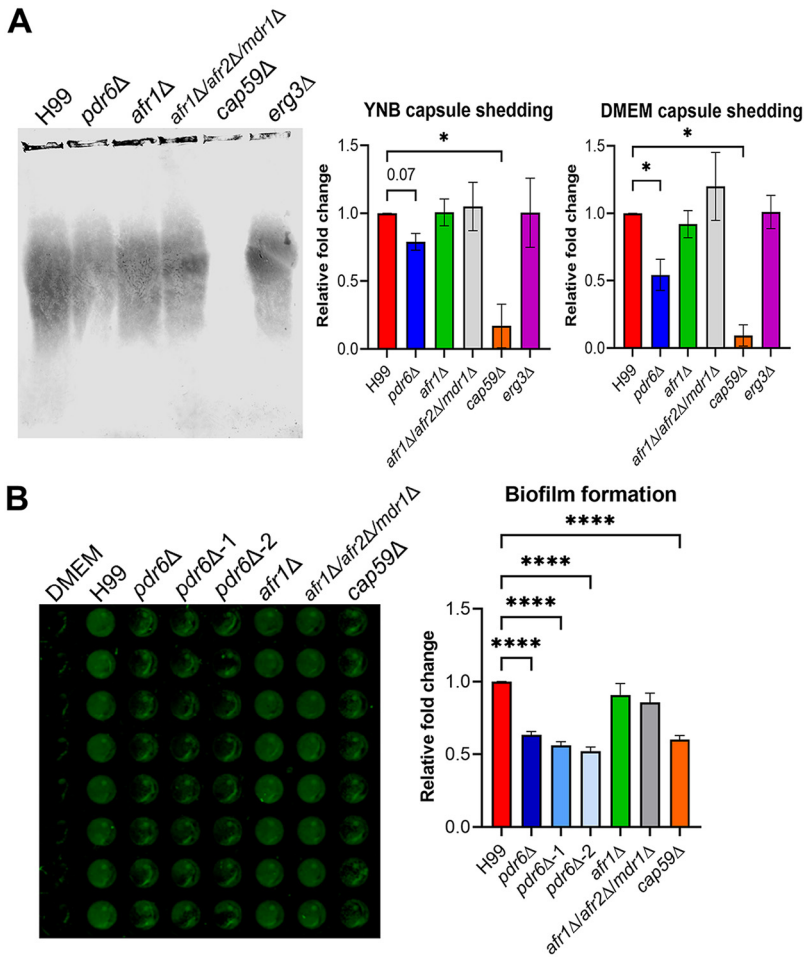

FIG 8 Deletion of *PDR6* alters capsular secretion and biofilm formation. (A) Capsule shedding assays were performed to determine the amount of GXM secreted from cryptococcal strains into the medium. Representative immunoblot showing shed GXM from cells grown for 2 days in YNB (left). Visualization of shed GXM was done using fluorescent detection (Odyssey, LiCor). Quantification of the signal revealed that the *pdr6*Δ mutant shed significantly less capsule than WT under DMEM (host-like) conditions and, albeit not statistically significant, there was a clear trend of less shedding in YNB conditions as well. Values from at least 3 independent experiments were normalized to the WT shed capsule and combined. Bars represent the mean ± SEM. (B) Biofilm-forming assays were performed in nontreated microtiter plates, incubated for 72 h, washed, and visualized for biofilms using a fluorescent imaging system (Odyssey, LiCor). Quantification of the signal revealed that all *pdr6*Δ mutants form weaker/fewer adherent biofilms compared to the WT. Values from at least 3 independent experiments were normalized to WT and combined. Bars represent mean ± SEM. Significance was determined using one-way ANOVA compared to H99 (Brown-Forsythe and Welch's corrected); *, $P < 0.05$; ****, $P < 0.0001$.

decreased capsule shedding, we next assessed its ability to survive within the challenging and harsh intracellular environment. To test this, we performed *in vitro* survival assays and found that the *pdr6*Δ mutant struggled to survive within host macrophages compared to the WT (Fig. 9A). After 4h in the presence of naïve human macrophages, ~10% of intracellular WT cells died, whereas 25% to 35% of the *pdr6*Δ cells are killed. To expand on this mild *in vitro* defect, we tested the virulence of the *pdr6*Δ mutant in a murine inhalation model of cryptococcosis, monitoring disease progression by weight loss. Infection with the WT strain resulted in all animals steadily losing weight by about 2 weeks, 50% of them dying in 17 days, and all succumbing to infection by day 19 (Fig. 9B). In contrast, mice infected with the original *pdr6*Δ and the recreated *pdr6*Δ-1 strains lived about 2 weeks longer than the WT-infected mice, with animals beginning to die at day 34, and all succumbing to infection by day 41, thus showing a significant increase in survival. Notably, CFU recovered from these mice at the time of death showed significantly less organ burden

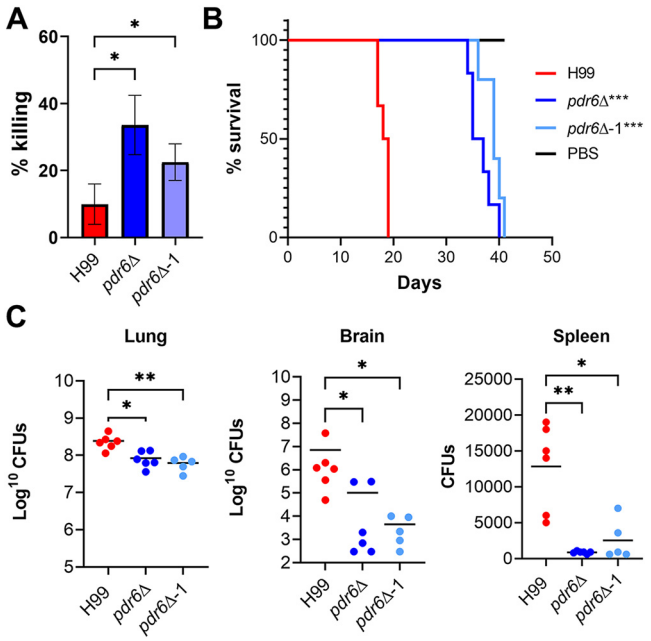

FIG 9 *pdr6*Δ mutant displays attenuated virulence *in vitro* and *in vivo*. (A) *In vitro* survival of H99 and *pdr6*Δ strains. Fungi and THP-1 cells were coincubated for 1 h at a multiplicity of infection (MOI) of 0.1 and washed to remove free cryptococci. Half the samples were lysed to determine intracellular fungi and the other half was grown for an additional 3 h, after which they were also lysed. Shown as the percentage killed, values represent the mean ± SEM from five independent experiments. Significance was determined using Repeated Measures (RM) one-way ANOVA compared to H99 (Geisser-Greenhouse correction); *, $P < 0.05$. (B) *In vivo* survival curve of H99 and *pdr6*Δ-infected mice. Five to six AJ/Cr mice per group were infected intranasally with 5×10^4 *C. neoformans*, or mock-infected with DPBS and monitored for up to 41 days (the experiment terminated when the last infected mouse died). Significance was determined using Mantel-Cox test; ***, $P < 0.001$. (C) Calculated organ burden of H99 and *pdr6*Δ strains at the time of death. Organs were harvested, homogenized, and dilutions were plated on YPD. Plates were incubated for 48 h and CFU was counted. Each data point represents a mouse and black bars represent the mean. There was a significantly less fungal burden in the lungs and a clear defect in dissemination. Significance was determined using a nonparametric one-way ANOVA with multiple comparisons (Dunn's corrected), *, $P < 0.05$.

compared to WT-infected mice, and a clear defect in dissemination to the brain and spleen (Fig. 9C), supporting an altered progression or attenuated pathology. Consistently, the *pdr6*Δ-infected mice exhibited respiratory symptoms (rapid and labored breathing) that were absent in the WT-infected mice, and their lungs were significantly more inflamed and enlarged than the WT lungs at the time of death. Taken together, these data suggest that *PDR6* function is required for full cryptococcal pathogenesis, and in its absence, the manifestation of the disease is protracted with altered symptomatology.

DISCUSSION

The H99 genome contains 10 genes encoding PDR-type ABC transporters (Fig. 1B and Text S1). Although it has a conserved representative gene in all clades except clade II, few have been characterized. Here, we present an initial characterization of an atypical, half-size, PDR transporter found in a fungal-host interaction screen. This gene, which we called *PDR6*, is conserved in the fungal kingdom (clade VIb), but no function has been reported for that subgroup. Because all the other members of that clade are pathogenic fungi, our work may have broad implications for medically important fungi. Given the similarity of *PDR6* to *AFR1* and *PDR5* (*AFR2*), which have been shown to act as efflux pumps for FLC, we tested the hypothesis that *PDR6* might act similarly. However, our data show that it is unlikely that Pdr6 is a major efflux pump for the compounds tested, including FLC. The *pdr6*Δ mutant accumulates the same level of all these compounds, yet it is hypersensitive to them.

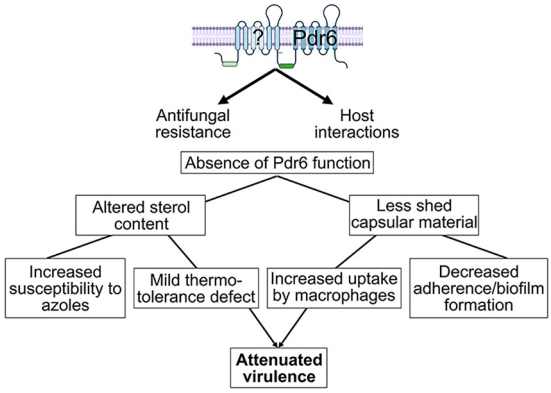

FIG 10 Model of Pdr6 and relationship to antifungal resistance, host interactions, and virulence. Pdr6 was a half-size transporter (dark blue), hence it needed to dimerize with itself or another half-size transporter (light blue) to be functional. In its absence, altered sterol content contributes to azole and thermal susceptibility, and the reduced capsule shedding promotes recognition and phagocytosis by host macrophages. Together, these phenotypes resulted in altered pathogenesis and attenuated virulence.

We then focused on ergosterol, the direct or indirect target of most antifungal drugs. Studies in the model yeast *S. cerevisiae* have documented the ergosterol biosynthetic pathway in detail (48). This occurs in the ER, yet how ergosterol is trafficked to the PM is not known, although it is known that vesicular trafficking is not involved (49). In this yeast, *PDR18* has been implicated in that process, and indeed, when *PDR6* is compared to the *S. cerevisiae* genome, *PDR18* is the gene closest to it, although there is no real *PDR6* homolog in *S. cerevisiae*. Moreover, fungal and plant PDR genes are part of the subfamily G of ABC transporters. In mammals, all ABCG members are half-size, and the mouse ABCG3 and human ABCG5 and ABCG8 transporters are all involved in cholesterol transport (50). Interestingly, BLAST analysis of these ABCG sequences against the *Cryptococcus* genome identifies *PDR6* as the gene with the highest similarity to ABCG3 and ABCG8. Hence, our finding that Pdr6-GFP localizes to the ER and the PM, the biosynthesis site and final destination of ergosterol, respectively, and that the *pdr6*Δ mutant has decreased ergosterol while the ADΔΔ+Pdr6-GFP increases PM ergosterol, strongly support a model were Pdr6 functions as an ergosterol transporter. Notably, this function seems not to be conserved in other PDR genes, as the *afr1*Δ and *afr1*Δ/*afr2*Δ/*mdr1*Δ mutants have normal levels of ergosterol as quantified by filipin staining. Interestingly, the *pdr6*Δ mutant is not more resistant to AMB as would be expected for strains lacking ergosterol (30), at least as judged by MIC values. A previous study of the susceptibility of young and old cells to AMB found that cells lacking *PDR6* were less resilient to AMB treatment, but this was measured as a percentage of survival and not as MIC values, preventing comparison of those results with ours (51). Overall, our data indicate that the diminished levels of ergosterol were low enough to promote sensitivity to azoles but high enough to still be targeted by AMB and exert its antifungal activity.

It is known that defects in the PM can affect the cell wall and/or capsule (52, 53). We did not find evidence for gross alterations to either of these layers, but the defect in capsule shedding, and the results of the CM studies, are highly suggestive of Pdr6 having a role in the regulated shedding of the capsule. It has been shown that the capsule is shed constitutively, but recent studies have demonstrated that capsule shedding can also be regulated (43). *PDR6* is highly and rapidly induced under host conditions, which are conditions known to induce capsule growth and shedding. Notably, it is known that normal levels of ergosterol are needed for thermotolerance. Hence, if *PDR6* is involved in ergosterol homeostasis, it would be expected to be induced upon shift to body temperature. The altered ergosterol levels in the *pdr6*Δ mutant could explain both the increased sensitivity to FLC and other azoles and the mild defect in thermotolerance (Fig. 10). However, low ergosterol cannot explain the reduced capsule shedding in this mutant as the *erg3*Δ mutant, which also has low levels of ergosterol, sheds similar amounts as WT. Additionally, other

ergosterol mutants have also been shown to shed normal levels of the capsule (30). This phenotype still needs more investigation.

Lastly, we show that Pdr6 function is needed for normal progression and disease manifestation in the mouse inhalational model. This could be explained by the decreased capsular shedding, high phagocytosis, and lower intracellular survival (Fig. 10). The increased recognition and phagocytosis could give the host an advantage because the fungus does not survive as well intracellularly. This would affect dissemination, as there is ample evidence that phagocytes are needed for extrapulmonary dissemination, a process known as trojan-horse transit (54). However, for trojan-horse transit to occur, the fungus must be able to survive intracellularly, and the *pdr6*Δ mutant is defective in this respect. Moreover, the decreased capsule shedding from the extracellular fungi would result in a stronger inflammatory response. The *pdr6*Δ mutant is also capable of inducing the production of a large capsule, hence, over time, fewer cells would be phagocytosed, and free cells in the tissue would accumulate. With the increased fungal burden, and the stronger inflammatory response, the host advantage is lost, and the animals die exhibiting different symptoms. Ongoing studies into the immunological response of the animals to *pdr6*Δ infection will shed more light on this hypothesis.

In conclusion, we have described a new mechanism by which cryptococcal cells can modulate their susceptibility to azoles: ergosterol transport regulated by Pdr6. Our results with the CM also indicate a potential new antiphagocytic mechanism: the *pdr6*Δ mutant can still grow a capsule, yet it is recognized and phagocytosed more avidly. Given that there are *PDR6* homologs in other fungal pathogens, it would be interesting to see if this function is conserved. Notably, a *PDR6* ortholog is missing in *C. deneoformans*, but present in *C. gattii*. *C. deneoformans* is considerably less pathogenic than *C. neoformans*, and *C. gattii* is considered a primary pathogen, although it is more associated with pneumonia than CNS infection. Would the absence of *PDR6* in *C. deneoformans* contribute to the virulence differences? Moreover, in addition to *PDR6*, *C. neoformans* has two additional half-size PDR transporters, which are missing in *C. gattii*. These are not in clade VIb, but their function is nevertheless unknown and could be related to Pdr6 because Pdr6 must homodimerize or heterodimerize to form a functional transporter. The binding partner of Pdr6 might influence the function of the resulting complex, which could be important under certain environmental conditions, such as inside a host. Elucidation of the diverse functions of ABC transporters, specifically the PDR-type, has the potential to open new lines of investigation for better treatments for this devastating disease.

MATERIALS AND METHODS

Strains, cell lines, growth conditions, and reagents. All *C. neoformans* strains used were in the serotype A strain H99α background. The original *pdr6*Δ strain was obtained from the Madhani deletion collection (55) and the recreated strains were made in this background by biolistics (see details below). H99α *afr1*Δ and H99α *afr1*Δ/*afr2*Δ/*mdr1*Δ were generous gifts from Yun Chang (National Institutes of Health). The *S. cerevisiae* strain ADΔΔ and the plasmids pABC3 and pABC3-KLmGH were graciously shared by Richard Cannon (Otago University, New Zealand). Maintenance and growth conditions, as well as medium details, can be found in Text S1.

The human monocyte cell line THP-1 (ATCC TIB-202) was grown in a THP-1 complete medium and differentiated with phorbol 12-myristate 12-acetate (PMA, Sigma) as described in (55). THP-1 cells were split every 3 to 4 days and new vials were thawed every month. Details on complete medium preparation and differentiation into macrophages can be found in Text S1.

All antifungals, xenobiotics, and other chemicals used were obtained through VWR or from Sigma. Details on the preparation of stock solutions, including solvent concentrations, as well as their storage information can be found in Text S1.

Fungal genome manipulation. Because complementation strains of the original *pdr6*Δ (from the Madhani collection) proved challenging to create, we used the split marker method (56) to delete the whole *PDR6* coding region in H99α after amplifying NAT resistance split marker fragments from genomic DNA of strain 1F1 (*pdr6*Δ) of the Madhani deletion collection. Three independent *pdr6*Δ mutant strains were generated to verify that all observed phenotypes are a direct result of the loss of *PDR6* (Fig. S2). Additionally, we performed whole-genome sequencing on the generated *pdr6*Δ mutants to confirm proper genetic manipulation (unpublished data).

Drug susceptibility assays. The CLSI M27-A3 reference method was used to determine the MIC of each drug (57). Briefly, the compounds to be tested were prepared at 2× the final concentration from stock solutions in RPMI 1640 medium. These were dispensed in a 96-well plate with 2-fold serial dilutions. Five hundred cells in the same volume as the drugs were then added to each well. Plates were

incubated at 37°C and 5% CO_2 for 48 to 72 h. MICs were quantified by measuring the optical density at 600 nm (OD_{600}) using a microtiter plate reader. For details on the compounds and concentration ranges tested see Text S1.

The MIC of FLC was also determined on RPMI plates with Epsilometer test strips (Etest strips; Liofilchem Thermo). Approximately 5×10^4 cells were plated on RPMI agar plates before application of the Etest strips. Plates were incubated at 30°C for 48 h.

Checkerboard assays. Checkerboard assays to assess the fractional inhibitory concentrations (FICs) for combinations of antifungal drugs were performed as previously described (58). Log phase cultures were used and mixed with the antifungal stocks in RPMI 1640. For more details on the procedure, final antifungal concentrations, and calculations of the FIC index, see Text S1. An FIC index value less than 0.5 was considered synergistic, additive if the value was between 1.0 and 0.5, and antagonistic if the FIC index was $\geq$2.0.

Flow cytometry analysis of the efflux of R6G, Nile Red, and Probe 1. Accumulation assays were performed as previously described (24, 34). Briefly, strains were grown overnight in Yeast extract-Peptone-Dextrose (YPD) at 30°C with shaking. Log-phase cultures were incubated with the fluorescent reporters in PBS for 30 min at 30°C with shaking. The reactions were stopped by cooling on ice, and the mixture was diluted 40-fold in cold 1× PBS. The accumulation was immediately assessed by flow cytometry. For details on the concentration of the reporters, the lasers and filters used, and how the data were analyzed see Text S1. Synthesis of Probe 1 was done in the Mobashery lab following published methods (34). For a detailed synthetic scheme and characterization of the product see Text S1.

Liquid chromatography/mass spectrometry (LC/MS). Log-phase cultures were incubated with FLC as above. A total of 200 μL was removed for CFU quantification and the rest was processed to make the lysate. The lysate was mixed with the same volume of cold MeOH, vortexed, and spun down. The supernatant was mixed with the same volume of CH_2Cl_2, vortexed, and spun down. The organic (bottom) phase was transferred into a glass tube, the solvent was evaporated, and the residues were resuspended in MeOH. At this point, the samples were further cleaned by passing through a solid-phase extraction (SPE) column. The elutes from SPE were concentrated by speedvac, reconstituted in 50:50 water:MeOH, and analyzed using LC/MS. For details on the instrumentation, columns, buffers, flow rates, software, and mass-spec parameters see Text S1.

Phenotyping. Strains tested were grown overnight in YPD, diluted to an OD_{600} of 0.2, and grown for two doublings. The cultures were diluted to 1×10^7 cells/mL and serially diluted (10-fold) and spotted (5 μL) onto YPD with 1 M NaCl, 0.005% SDS, 0.1% Congo red, and 0.5 μg/mL caffeine. Plates were incubated at 30°C for 48 to 72 h.

Uptake assay. Uptake assays were performed as previously described (26). Briefly, differentiated THP-1 cells were incubated with Lucifer Yellow-stained fungal cells that had been opsonized with 40% fresh human serum obtained from healthy donors (approved by the University of Notre Dame Institutional Review Board (IRB) as a non-human subject research procedure). Following a 1 h incubation, the plates were washed using a microplate washer (405LS, Biotek, Winooski, VT), fixed with 4% formaldehyde, and stained with DAPI (Sigma) and CellMask Deep Red (Invitrogen). NaN_3 in PBS was added to the plates and images were obtained using a Zeiss Axio Observer microscope, equipped with an automated stage. Each well was automatically imaged in a 3 × 3 grid and the images were analyzed using a Cell Profiler pipeline to determine phagocytic index (PI) values. For more details on these procedures, including the Cell Profiler pipeline, see Text S1.

Conditioned medium. Conditioned medium (CM) was generated as previously described (59). Briefly, overnight cultures were diluted to 1×10^5 cells/mL in RPMI 1640 medium and incubated for 5 days at 30°C. Cells were removed by centrifugation and the supernatant was filtered through a 0.25-μm filter.

Capsule induction. Cells were grown overnight in YPD, washed with DMEM, and 1×10^6 cells/mL were added to 24-well tissue culture plates. Plates were incubated at 37°C and 5% CO_2 for 24 h. The cell suspension was collected and washed, India ink was added, and samples were visualized on a Zeiss microscope. Images were analyzed with ImageJ (NIH) for capsule thickness.

Capsule shedding assay. Capsule shedding assays were performed as previously described (43, 44). Briefly, strains were grown overnight in YPD at 30°C, washed, and diluted to 1×10^6 cells/mL in DMEM. Following a 15 h incubation at 37°C and 5% CO_2, the samples were heated to denature enzymes, centrifuged to separate cells and supernatant, and then stored at 4°C. The samples were loaded on a 0.6% certified megabase agarose (Bio-Rad) gel and subjected to electrophoresis for 15 h at 25 V. Gel contents were transferred to a positively charged membrane using a standard Southern blot protocol with 10× SSC. Following the overnight transfer, the membrane was blocked for 48 h in 1× TBS-5% milk and incubated for 1 h in 1× TBST-1% milk with 1 μg/mL of anti-GXM monoclonal antibody. The membrane was rinsed three times in 1× TBST and incubated for 1 h in 1× TBST-1% milk with Odyssey antibody at 1:10,000. The membrane was rinsed again three times in 1× TBST and imaged on the Odyssey (Licor).

Biofilm/adherence assay. Cryptococcal adherence assays were performed in nontreated 96-well plates (CLS3631, Corning). Briefly, strains were grown overnight in YPD, diluted to 1×10^7 cells/mL in DMEM, and 100 μL of cell suspension was added to the wells. Plates were incubated at 37°C and 5% CO_2 for 72 h, washed with PBS, fixed with 4% formaldehyde, blocked with 1.5% BSA and 0.1% NaN_3 in PBS, and incubated with anti-GXM primary and secondary antibodies. Plates were imaged on the Odyssey and quantified using ImageStudio software.

Biofilms were also quantified by the XTT reduction assay, as previously described (60, 61). For details on this assay see Text S1.

Filipin staining. Staining of membrane sterols was performed as previously described (36, 62). Briefly, log-phase cultures grown in YPD were stained for 5 min with 5 μg/mL of filipin (Sigma) and washed with PBS. After washing cells were immediately visualized with an inverted Zeiss microscope. Fluorescence was calculated using

Cell Profiler software. Additionally, fluorescent levels were quantified with a fluorescent plate reader (Bio-Tek). Fluorescence was measured at the range of 360 to 470 nm wavelength and normalized by OD_{600}.

Mouse virulence studies. To test virulence in a murine model, strains were cultured overnight in YPD, collected, washed, and diluted to 10^6 cells/mL in DPBS. 50 μL of the cell suspension (or DPBS for the mock-infected) was used to intranasally inoculate groups of five mice (5 to 6-week-old female A/Jcr mice; Jackson Laboratories). Animals were closely monitored and sacrificed if they lost >20% relative to peak weight or at the end of the experiment (41 days). Homogenates of lungs, brains, and spleens were plated to determine organ burden.

SUPPLEMENTAL MATERIAL

Supplemental material is available online only.

TEXT S1, DOCX file, 0.1 MB.

FIG S1, TIF file, 0.8 MB.

FIG S2, TIF file, 1.4 MB.

ACKNOWLEDGMENTS

We acknowledge assistance and support for the LC-MS by Mijoon Lee from the Notre Dame Mass Spectrometry Core. We acknowledge financial support from the Warren Center for Drug Discovery for a Sean Cocchia Rare Disease Research seed grant.

Y.Q. is a Fellow of the Chemistry–Biochemistry–Biology Interface Program at the University of Notre Dame, supported by Training Grant T32 GM075762 from the National Institutes of Health. Y.Q. was also an ECK Institute for Global Health Fellow at the University of Notre Dame.

We thank Richard Cannon for their gift of the ADΔΔ strain and associated plasmids. We also thank members of the Santiago-Tirado lab for thoughtful comments and feedback on this work.

We declare no conflict of interest.

REFERENCES

1. Higgins CF. 2001. ABC transporters: physiology, structure and mechanism–an overview. Res Microbiol 152:205–210. https://doi.org/10.1016/s0923-2508(01)01193-7.
2. Jungwirth H, Kuchler K. 2006. Yeast ABC transporters– a tale of sex, stress, drugs and aging. FEBS Lett 580:1131–1138. https://doi.org/10.1016/j.febslet.2005.12.050.
3. Holland IB, Cole SPC, Kuchler K, Higgins CF. 2003. ABC Proteins from bacteria to man. Academic Press, Amsterdam.
4. Khunweeraphong N, Kuchler K. 2021. Multidrug resistance in mammals and fungi-from MDR to PDR: a rocky road from atomic structures to transport mechanisms. Int J Mol Sci 22:4806. https://doi.org/10.3390/ijms22094806.
5. Lamping E, Baret PV, Holmes AR, Monk BC, Goffeau A, Cannon RD. 2010. Fungal PDR transporters: phylogeny, topology, motifs and function. Fungal Genet Biol 47:127–142. https://doi.org/10.1016/j.fgb.2009.10.007.
6. Bongomin F, Gago S, Oladele RO, Denning DW. 2017. Global and multinational prevalence of fungal diseases-estimate precision. J Fungal (Basel) 3:57. https://doi.org/10.3390/jof3040057.
7. Niimi M, Tanabe K, Wada S, Yamazaki A, Uehara Y, Niimi K, Lamping E, Holmes AR, Monk BC, Cannon RD. 2005. ABC transporters of pathogenic fungi: recent advances in functional analyses. Nihon Ishinkin Gakkai Zasshi 46:249–260. https://doi.org/10.3314/jjmm.46.249.
8. Kovalchuk A, Driessen AJ. 2010. Phylogenetic analysis of fungal ABC transporters. BMC Genomics 11:177. https://doi.org/10.1186/1471-2164-11-177.
9. May RC, Stone NR, Wiesner DL, Bicanic T, Nielsen K. 2016. Cryptococcus: from environmental saprophyte to global pathogen. Nat Rev Microbiol 14:106–117. https://doi.org/10.1038/nrmicro.2015.6.
10. Rajasingham R, Smith RM, Park BJ, Jarvis JN, Govender NP, Chiller TM, Denning DW, Loyse A, Boulware DR. 2017. Global burden of disease of HIV-associated cryptococcal meningitis: an updated analysis. Lancet Infect Dis 17:873–881. https://doi.org/10.1016/S1473-3099(17)30243-8.
11. Coelho C, Casadevall A. 2016. Cryptococcal therapies and drug targets: the old, the new and the promising. Cell Microbiol 18:792–799. https://doi.org/10.1111/cmi.12590.
12. Zhang J, Li L, Lv Q, Yan L, Wang Y, Jiang Y. 2019. The fungal CYP51s: their functions, structures, related drug resistance, and inhibitors. Front Microbiol 10:691. https://doi.org/10.3389/fmicb.2019.00691.
13. Atim PB, Meya DM, Gerlach ES, Muhanguzi D, Male A, Kanamwanji B, Nielsen K. 2022. Lack of association between fluconazole susceptibility and ERG11 nucleotide polymorphisms in Cryptococcus neoformans clinical isolates from Uganda. JoF 8:508. https://doi.org/10.3390/jof8050508.
14. Hope W, Stone NRH, Johnson A, McEntee L, Farrington N, Santoro-Castelazo A, Liu X, Lucaci A, Hughes M, Oliver JD, Giamberardino C, Mfinanga S, Harrison TS, Perfect JR, Bicanic T. 2019. Fluconazole monotherapy is a suboptimal option for initial treatment of cryptococcal meningitis because of emergence of resistance. mBio 10:e02575-19. https://doi.org/10.1128/mBio.02575-19.
15. Moreira IMB, Cortez ACA, de Souza ES, Pinheiro SB, de Souza Oliveira JG, Sadahiro A, Cruz KS, Matsuura ABJ, Melhem MSC, Frickmann H, de Souza JVB. 2022. Investigation of fluconazole heteroresistance in clinical and environmental isolates of Cryptococcus neoformans complex and Cryptococcus gattii complex in the state of Amazonas. Brazil Med Mycol 60:myac005. https://doi.org/10.1093/mmy/myac005.
16. Yang C, Bian Z, Blechert O, Deng F, Chen H, Li Y, Yang Y, Chen M, Zhan P. 2021. High prevalence of HIV-related Cryptococcosis and increased resistance to fluconazole of the Cryptococcus neoformans complex in Jiangxi Province, South Central China. Front Cell Infect Microbiol 11:723251. https://doi.org/10.3389/fcimb.2021.723251.
17. Sionov E, Chang YC, Garraffo HM, Dolan MA, Ghannoum MA, Kwon-Chung KJ. 2012. Identification of a Cryptococcus neoformans cytochrome P450 lanosterol 14alpha-demethylase (Erg11) residue critical for differential susceptibility between fluconazole/voriconazole and itraconazole/posaconazole. Antimicrob Agents Chemother 56:1162–1169. https://doi.org/10.1128/AAC.05502-11.
18. Rodero L, Mellado E, Rodriguez AC, Salve A, Guelfand L, Cahn P, Cuenca-Estrella M, Davel G, Rodriguez-Tudela JL. 2003. G484S amino acid substitution in lanosterol 14-alpha demethylase (ERG11) is related to fluconazole resistance in a recurrent Cryptococcus neoformans clinical isolate. Antimicrob Agents Chemother 47:3653–3656. https://doi.org/10.1128/AAC.47.11.3653-3656.2003.
19. Bennett RJ, Forche A, Berman J. 2014. Rapid mechanisms for generating genome diversity: whole ploidy shifts, aneuploidy, and loss of

heterozygosity. Cold Spring Harb Perspect Med 4:a019604. https://doi.org/10.1101/cshperspect.a019604.
20. Stone NR, Rhodes J, Fisher MC, Mfinanga S, Kivuyo S, Rugemalila J, Segal ES, Needleman L, Molloy SF, Kwon-Chung J, Harrison TS, Hope W, Berman J, Bicanic T. 2019. Dynamic ploidy changes drive fluconazole resistance in human cryptococcal meningitis. J Clin Invest 129:999–1014. https://doi.org/10.1172/JCI124516.
21. Holmes AR, Cardno TS, Strouse JJ, Ivnitski-Steele I, Keniya MV, Lackovic K, Monk BC, Sklar LA, Cannon RD. 2016. Targeting efflux pumps to overcome antifungal drug resistance. Future Med Chem 8:1485–1501. https://doi.org/10.4155/fmc-2016-0050.
22. Posteraro B, Sanguinetti M, Sanglard D, La Sorda M, Boccia S, Romano L, Morace G, Fadda G. 2003. Identification and characterization of a Cryptococcus neoformans ATP binding cassette (ABC) transporter-encoding gene, CnAFR1, involved in the resistance to fluconazole. Mol Microbiol 47:357–371. https://doi.org/10.1046/j.1365-2958.2003.03281.x.
23. Sanguinetti M, Posteraro B, La Sorda M, Torelli R, Fiori B, Santangelo R, Delogu G, Fadda G. 2006. Role of AFR1, an ABC transporter-encoding gene, in the in vivo response to fluconazole and virulence of Cryptococcus neoformans. Infect Immun 74:1352–1359. https://doi.org/10.1128/IAI.74.2.1352-1359.2006.
24. Chang M, Sionov E, Khanal Lamichhane A, Kwon-Chung KJ, Chang YC. 2018. Roles of three Cryptococcus neoformans and Cryptococcus gattii efflux pump-coding genes in response to drug treatment. Antimicrob Agents Chemother 62:e01751-17. https://doi.org/10.1128/AAC.01751-17.
25. Ko YJ, Yu YM, Kim GB, Lee GW, Maeng PJ, Kim S, Floyd A, Heitman J, Bahn YS. 2009. Remodeling of global transcription patterns of Cryptococcus neoformans genes mediated by the stress-activated HOG signaling pathways. Eukaryot Cell 8:1197–1217. https://doi.org/10.1128/EC.00120-09.
26. Santiago-Tirado FH, Peng T, Yang M, Hang HC, Doering TL. 2015. A Single protein S-acyl transferase acts through diverse substrates to determine cryptococcal morphology, stress tolerance, and pathogenic outcome. PLoS Pathog 11:e1004908. https://doi.org/10.1371/journal.ppat.1004908.
27. Inglis DO, Skrzypek MS, Liaw E, Moktali V, Sherlock G, Stajich JE. 2014. Literature-based gene curation and proposed genetic nomenclature for cryptococcus. Eukaryot Cell 13:878–883. https://doi.org/10.1128/EC.00083-14.
28. Velamakanni S, Wei SL, Janvilisri T, van Veen HW. 2007. ABCG transporters: structure, substrate specificities and physiological roles: a brief overview. J Bioenerg Biomembr 39:465–471. https://doi.org/10.1007/s10863-007-9122-x.
29. Neumann S, Hartmann H, Martin-Galiano AJ, Fuchs A, Frishman D. 2012. Camps 2.0: exploring the sequence and structure space of prokaryotic, eukaryotic, and viral membrane proteins. Proteins 80:839–857. https://doi.org/10.1002/prot.23242.
30. Oliveira FFM, Paes HC, Peconick LDF, Fonseca FL, Marina CLF, Bocca AL, Homem-de-Mello M, Rodrigues ML, Albuquerque P, Nicola AM, Alspaugh JA, Felipe MSS, Fernandes L. 2020. Erg6 affects membrane composition and virulence of the human fungal pathogen Cryptococcus neoformans. Fungal Genet Biol 140:103368. https://doi.org/10.1016/j.fgb.2020.103368.
31. Brown HE, Telzrow CL, Saelens JW, Fernandes L, Alspaugh JA. 2020. Sterol-response pathways mediate alkaline survival in diverse fungi. mBio 11:e00719-20. https://doi.org/10.1128/mBio.00719-20.
32. Kolaczkowski M, van der Rest M, Cybularz-Kolaczkowska A, Soumillion JP, Konings WN, Goffeau A. 1996. Anticancer drugs, ionophoric peptides, and steroids as substrates of the yeast multidrug transporter Pdr5p. J Biol Chem 271:31543–31548. https://doi.org/10.1074/jbc.271.49.31543.
33. Ivnitski-Steele I, Holmes AR, Lamping E, Monk BC, Cannon RD, Sklar LA. 2009. Identification of Nile red as a fluorescent substrate of the Candida albicans ATP-binding cassette transporters Cdr1p and Cdr2p and the major facilitator superfamily transporter Mdr1p. Anal Biochem 394:87–91. https://doi.org/10.1016/j.ab.2009.07.001.
34. Benhamou RI, Bibi M, Steinbuch KB, Engel H, Levin M, Roichman Y, Berman J, Fridman M. 2017. Real-time imaging of the azole class of antifungal drugs in live candida cells. ACS Chem Biol 12:1769–1777. https://doi.org/10.1021/acschembio.7b00339.
35. Paul S, Kannan I, Mohanram K. 2019. Extensive ERG11 mutations associated with fluconazole-resistant Candida albicans isolated from HIV-infected patients. Curr Med Mycol 5:1–6. https://doi.org/10.18502/cmm.5.3.1739.
36. Altamirano S, Simmons C, Kozubowski L. 2018. Colony and single cell level analysis of the heterogeneous response of cryptococcus neoformans to fluconazole. Front Cell Infect Microbiol 8:203. https://doi.org/10.3389/fcimb.2018.00203.
37. Godinho CP, Prata CS, Pinto SN, Cardoso C, Bandarra NM, Fernandes F, Sa-Correia I. 2018. Pdr18 is involved in yeast response to acetic acid stress counteracting the decrease of plasma membrane ergosterol content and order. Sci Rep 8:7860. https://doi.org/10.1038/s41598-018-26128-7.
38. Godinho CP, Costa R, Sa-Correia I. 2021. The ABC transporter Pdr18 is required for yeast thermotolerance due to its role in ergosterol transport and plasma membrane properties. Environ Microbiol 23:69–80. https://doi.org/10.1111/1462-2920.15253.
39. Lamping E, Monk BC, Niimi K, Holmes AR, Tsao S, Tanabe K, Niimi M, Uehara Y, Cannon RD. 2007. Characterization of three classes of membrane proteins involved in fungal azole resistance by functional hyperexpression in Saccharomyces cerevisiae. Eukaryot Cell 6:1150–1165. https://doi.org/10.1128/EC.00091-07.
40. Madani G, Lamping E, Lee HJ, Niimi M, Mitra AK, Cannon RD. 2021. Small-scale plasma membrane preparation for the analysis of Candida albicans Cdr1-mGFPHis. J Vis Exp 172.
41. Gaylord EA, Choy HL, Doering TL. 2020. Dangerous liaisons: interactions of Cryptococcus neoformans with host phagocytes. Pathogens 9:891. https://doi.org/10.3390/pathogens9110891.
42. Zaragoza O, Rodrigues ML, De Jesus M, Frases S, Dadachova E, Casadevall A. 2009. The capsule of the fungal pathogen Cryptococcus neoformans. Adv Appl Microbiol 68:133–216. https://doi.org/10.1016/S0065-2164(09)01204-0.
43. Denham ST, Verma S, Reynolds RC, Worne CL, Daugherty JM, Lane TE, Brown JCS. 2018. Regulated release of cryptococcal polysaccharide drives virulence and suppresses immune cell infiltration into the central nervous system. Infect Immun 86:e00662-17. https://doi.org/10.1128/IAI.00662-17.
44. Yoneda A, Doering TL. 2008. Regulation of Cryptococcus neoformans capsule size is mediated at the polymer level. Eukaryot Cell 7:546–549. https://doi.org/10.1128/EC.00437-07.
45. Martinez LR, Casadevall A. 2015. Biofilm formation by Cryptococcus neoformans. Microbiol Spectr 3. https://doi.org/10.1128/microbiolspec.MB-0006-2014.
46. Lee HH, Del Pozzo J, Salamanca SA, Hernandez H, Martinez LR. 2019. Reduced phagocytosis and killing of Cryptococcus neoformans biofilm-derived cells by J774.16 macrophages is associated with fungal capsular production and surface modification. Fungal Genet Biol 132:103258. https://doi.org/10.1016/j.fgb.2019.103258.
47. Ravi S, Pierce C, Witt C, Wormley FL, Jr. 2009. Biofilm formation by Cryptococcus neoformans under distinct environmental conditions. Mycopathologia 167:307–314. https://doi.org/10.1007/s11046-008-9180-6.
48. Jorda T, Puig S. 2020. Regulation of ergosterol biosynthesis in Saccharomyces cerevisiae. Genes (Basel) 11:795. https://doi.org/10.3390/genes11070795.
49. Baumann NA, Sullivan DP, Ohvo-Rekila H, Simonot C, Pottekat A, Klaassen Z, Beh CT, Menon AK. 2005. Transport of newly synthesized sterol to the sterol-enriched plasma membrane occurs via nonvesicular equilibration. Biochemistry 44:5816–5826. https://doi.org/10.1021/bi048296z.
50. Kerr ID, Hutchison E, Gerard L, Aleidi SM, Gelissen IC. 2021. Mammalian ABCG-transporters, sterols and lipids: to bind perchance to transport? Biochim Biophys Acta Mol Cell Biol Lipids 1866:158860. https://doi.org/10.1016/j.bbalip.2020.158860.
51. Orner EP, Zhang P, Jo MC, Bhattacharya S, Qin L, Fries BC. 2019. High-throughput yeast aging analysis for Cryptococcus (HYAAC) microfluidic device streamlines aging studies in Cryptococcus neoformans. Commun Biol 2:256. https://doi.org/10.1038/s42003-019-0504-5.
52. Kumar P, Heiss C, Santiago-Tirado FH, Black I, Azadi P, Doering TL. 2014. Pbx proteins in Cryptococcus neoformans cell wall remodeling and capsule assembly. Eukaryot Cell 13:560–571. https://doi.org/10.1128/EC.00290-13.
53. Reese AJ, Doering TL. 2003. Cell wall alpha-1,3-glucan is required to anchor the Cryptococcus neoformans capsule. Mol Microbiol 50:1401–1409. https://doi.org/10.1046/j.1365-2958.2003.03780.x.
54. Santiago-Tirado FH, Doering TL. 2017. False friends: phagocytes as Trojan horses in microbial brain infections. PLoS Pathog 13:e1006680. https://doi.org/10.1371/journal.ppat.1006680.
55. Liu OW, Chun CD, Chow ED, Chen C, Madhani HD, Noble SM. 2008. Systematic genetic analysis of virulence in the human fungal pathogen Cryptococcus neoformans. Cell 135:174–188. https://doi.org/10.1016/j.cell.2008.07.046.
56. Fu J, Hettler E, Wickes BL. 2006. Split marker transformation increases homologous integration frequency in Cryptococcus neoformans. Fungal Genet Biol 43:200–212. https://doi.org/10.1016/j.fgb.2005.09.007.
57. CLSI. 2017. Reference Method for Broth Dilution Antifungal Susceptibility Testing of Yeasts. 4th ed CLSI Standard M27. Clinical and Laboratory Standard Institute, Wayne, PA.

58. Franzot SP, Casadevall A. 1997. Pneumocandin L-743,872 enhances the activities of amphotericin B and fluconazole against Cryptococcus neoformans in vitro. Antimicrob Agents Chemother 41:331–336. https://doi.org/10.1128/AAC.41.2.331.
59. Albuquerque P, Nicola AM, Nieves E, Paes HC, Williamson PR, Silva-Pereira I, Casadevall A. 2013. Quorum sensing-mediated, cell density-dependent regulation of growth and virulence in Cryptococcus neoformans. mBio 5:e00986-13–e00913. https://doi.org/10.1128/mBio.00986-13.
60. Pierce CG, Uppuluri P, Tristan AR, Wormley FL, Jr., Mowat E, Ramage G, Lopez-Ribot JL. 2008. A simple and reproducible 96-well plate-based method for the formation of fungal biofilms and its application to antifungal susceptibility testing. Nat Protoc 3:1494–1500. https://doi.org/10.1038/nprot.2008.141.
61. Martinez LR, Casadevall A. 2005. Specific antibody can prevent fungal biofilm formation and this effect correlates with protective efficacy. Infect Immun 73:6350–6362. https://doi.org/10.1128/IAI.73.10.6350-6362.2005.
62. Bang S, Kwon H, Hwang HS, Park KD, Kim SU, Bahn YS. 2014. 9-O-butyl-13–(4-isopropylbenzyl)berberine, KR-72, is a potent antifungal agent that inhibits the growth of Cryptococcus neoformans by regulating gene expression. PLoS One 9:e109863. https://doi.org/10.1371/journal.pone.0109863.